

Arbitrary-order all-fiber temporal differentiator based on a fiber Bragg grating: design and experimental demonstration

Ming Li¹, Davide Janner², Jianping Yao^{1*}, and Valerio Pruneri^{2,3}

¹*Microwave Photonics Research Laboratory, School of Information Technology and Engineering
University of Ottawa, Ottawa, ON, K1N 6N5, Canada*

²*ICFO-Institut de Ciències Fotoniques, Mediterranean Technology Park, 08860 Castelldefels, Spain*

³*ICREA - Institució Catalana de Recerca i Estudis Avançats, 08010, Barcelona, Spain.*

*jpyao@site.uOttawa.ca

Abstract: A new technique to design an all-fiber temporal differentiator that has a large bandwidth and an arbitrary differentiation order is proposed and investigated. The proposed temporal differentiator is a special fiber Bragg grating (FBG) that is designed by controlling its magnitude and phase responses with the discrete layer peeling (DLP) method. There are three important features of this technique: 1) the temporal differentiator has an arbitrary magnitude response and a controllable bandwidth; 2) the temporal differentiator can be designed and fabricated with an arbitrary differentiation order that is realized in a single FBG; 3) the required maximum index modulation of the FBG-based differentiator is largely decreased by using a Gaussian windowing function. The use of the proposed technique to design temporal differentiators with a differentiation order up to the fourth and with a bandwidth up to 500 GHz is studied. A proof-of-concept experiment is then carried out. A first- and a second-order temporal differentiator with a bandwidth of 25 GHz are experimentally demonstrated.

©2009 Optical Society of America

OCIS codes: (070.1170) Analog optical signal processing; (350.2770) Gratings; (070.7145) Ultrafast processing.

References and links

1. L. Venema, "Photonics Technologies," *Nature Insight* **424**, 809 (2003).
2. N. Q. Ngo, S. F. Yu, S. C. Tjin, and C. H. Kam, "A new theoretical basis of higher-derivative optical differentiators," *Opt. Commun.* **230**(1-3), 115–129 (2004).
3. M. Kulishov, and J. Azaña, "Long-period fiber gratings as ultrafast optical differentiators," *Opt. Lett.* **30**(20), 2700–2702 (2005).
4. R. Slavík, Y. Park, M. Kulishov, R. Morandotti, and J. Azaña, "Ultrafast all-optical differentiators," *Opt. Express* **14**(22), 10699–10707 (2006), <http://www.opticsinfobase.org/oe/abstract.cfm?URI=oe-14-22-10699>.
5. R. Slavík, Y. Park, N. Ayotte, S. Doucet, T. J. Ahn, S. LaRochelle, and J. Azaña, "Photonic temporal integrator for all-optical computing," *Opt. Express* **16**(22), 18202–18214 (2008), <http://www.opticsinfobase.org/abstract.cfm?URI=oe-16-22-18202>.
6. Q. Wang, F. Zeng, S. Blais, and J. Yao, "Optical ultrawideband monocycle pulse generation based on cross-gain modulation in a semiconductor optical amplifier," *Opt. Lett.* **31**(21), 3083–3085 (2006).
7. J. Xu, X. Zhang, J. Dong, D. Liu, and D. Huang, "All-optical differentiator based on cross-gain modulation in semiconductor optical amplifier," *Opt. Lett.* **32**(20), 3029–3031 (2007).
8. J. Xu, X. Zhang, J. Dong, D. Liu, and D. Huang, "High-speed all-optical differentiator based on a semiconductor optical amplifier and an optical filter," *Opt. Lett.* **32**(13), 1872–1874 (2007).
9. N. K. Berger, B. Levit, B. Fischer, M. Kulishov, D. V. Plant, and J. Azaña, "Temporal differentiation of optical signals using a phase-shifted fiber Bragg grating," *Opt. Express* **15**(2), 371–381 (2007), <http://www.opticsinfobase.org/oe/abstract.cfm?URI=oe-15-2-371>.
10. F. Liu, T. Wang, L. Qiang, T. Ye, Z. Zhang, M. Qiu, and Y. Su, "Compact optical temporal differentiator based on silicon microring resonator," *Opt. Express* **16**(20), 15880–15886 (2008), <http://www.opticsinfobase.org/oe/abstract.cfm?URI=oe-16-20-15880>.
11. L.-M. Rivas, K. Singh, A. Carballar, and J. Azaña, "Arbitrary-order ultra-broadband all-optical differentiators based on fiber Bragg gratings," *IEEE Photon. Technol. Lett.* **19**(16), 1209–1211 (2007).

12. L. M. Rivas, S. Boudreau, Y. Park, R. Slavík, S. Laroche, A. Carballar, and J. Azaña, "Experimental demonstration of ultrafast all-fiber high-order photonic temporal differentiators," *Opt. Lett.* **34**(12), 1792–1794 (2009).
13. M. A. Preciado, and M. A. Muriel, "Design of an ultrafast all-optical differentiator based on a fiber Bragg grating in transmission," *Opt. Lett.* **33**(21), 2458–2460 (2008).
14. R. Slavík, Y. Park, and J. Azaña, "Tunable dispersion-tolerant picosecond flat-top waveform generation using an optical differentiator," *Opt. Express* **15**(11), 6717–6726 (2007), <http://www.opticsinfobase.org/oe/abstract.cfm?URI=oe-15-11-6717>.
15. Y. Park, J. Azaña, and R. Slavík, "Ultrafast all-optical first- and higher-order differentiators based on interferometers," *Opt. Lett.* **32**(6), 710–712 (2007).
16. S. W. James, and R. P. Tatam, "Optical fibre long-period grating sensors: characteristics and application," *Meas. Sci. Technol.* **14**(5), R49–R61 (2003).
17. R. Feded, M. N. Zervas, and M. A. Muriel, "An efficient inverse scattering algorithm for the design of nonuniform fiber Bragg gratings," *IEEE J. Quantum Electron.* **35**(8), 1105–1115 (1999).
18. J. Skaar, L. Wang, and T. Erdogan, "On the synthesis of fiber Bragg grating by layer peeling," *IEEE J. Quantum Electron.* **37**(2), 165–173 (2001).
19. H. Li, T. Kumagai, K. Ogusu, and Y. Sheng, "Advanced design of a multichannel fiber Bragg grating based on a layer-peeling method," *J. Opt. Soc. Am. B* **21**, 1929–1938 (2004).
20. M. H. Asghari, and J. Azaña, "On the design of efficient and accurate arbitrary-order temporal optical integrators using fiber bragg gratings," *J. Lightwave Technol.* (to be published).
21. M. Bernier, Y. Sheng, and R. Vallée, "Ultrabroadband fiber Bragg gratings written with a highly chirped phase mask and infrared femtosecond pulses," *Opt. Express* **17**(5), 3285–3290 (2009), <http://www.opticsinfobase.org/abstract.cfm?URI=oe-17-5-3285>.
22. M. J. Cole, W. H. Loh, R. I. Laming, M. N. Zervas, and S. Barcelos, "Moving fibre/phase mask-scanning beam technique for enhanced flexibility in producing fibre gratings with uniform phase mask," *Electron. Lett.* **31**(17), 1488–1489 (1995).

1. Introduction

Recently, with the rapid development of photonics technologies, the implementations of basic operations with optics have attracted great interests due to the high potential to increase the signal processing speed that is several orders of magnitude higher than that achievable by digital electronics. A few fundamental all-optical operators, such as a photonic temporal differentiator and integrator, have been designed and practically realized [1–5]. A temporal differentiator is a basic operator that performs real-time differentiation of an optical signal in the optical domain. Usually, a temporal differentiator can be realized based on cross-gain modulation in a semiconductor optical amplifier (SOA) [6–8]. A temporal differentiation can also be realized using an optical filter, such as a π -phase shifted fiber Bragg grating (PS-FBG), a long period fiber grating (LPG), an optical interferometer, or a silicon micro-ring resonator [3–5,9–15]. In general, the reported temporal differentiators can be classified into two categories: incoherent optical differentiators that operate on the optical intensity of the input signal and coherent optical differentiators that operate on the complex field of the input signal. The differentiators reported in [6–8] are incoherent optical differentiators, and in [3–5,9–15] are coherent optical differentiators.

Among the techniques, an LPG-based differentiator has the advantage of a large bandwidth which allows the implementation of temporal differentiation of a broadband optical signal with a bandwidth up to a terahertz [4]. However, due to the coupling between the cladding and the core modes, an LPG-based differentiator is very sensitive to environmental changes. An FBG-based differentiator, however, has a comparatively higher tolerance to the environmental changes [16]. In addition, the transmission spectrum of an LPG is more difficult to be tailored as compared to that of an FBG. Indeed, the bandwidth of a PS-FBG is fairly narrow and it can only work for an optical signal with a bandwidth of about 10 GHz [9,10], Rivas et al. proposed a method to implement an arbitrary-order temporal differentiator based on a simple but specially apodized linearly chirped FBG (LC-FBG) working in transmission [11]. In this case, the temporal differentiation of an optical signal with a bandwidth up to a few hundred GHz can be realized. Very recently, an apodized LC-FBG cascaded with an LPG-based first-order differentiator is experimentally demonstrated to implement an arbitrary-order photonic temporal differentiator [10]. The reported temporal differentiator can operate up to the fourth order with a wide operation bandwidth up to the terahertz regime. The major limitation of this technique is that an additional FBG with a π -

phase shift or an LPG-based first-order differentiator that is cascaded with an apodized LC-FBG is required to implement odd-order differentiation. To reduce the complexity, Preciado and Muriel proposed a method to design an ultrafast all-optical first-order differentiator using a single FBG in transmission [13]. The π -phase shift is approximately generated by imposing a very high transmission dip. Due to the requirement for a very high transmission dip, the FBG usually has a long length and an extremely high coupling coefficient, which would make the FBG fabrication very challenging [13]. In addition, the magnitude response has a Lorentzian shape, which makes the differentiation bandwidth in-use much less than the bandwidth of the magnitude response.

In this paper, an arbitrary-order all-fiber temporal differentiator that has a large bandwidth designed with the discrete layer peeling (DLP) method is investigated. The DLP method was proposed by Feced and Skaar for the synthesis of an FBG that is able to efficiently and accurately reconstruct the grating structure from any given reflection spectrum [17–19]. Recently, this method has been employed to design an arbitrary-order temporal integrator [20]. In this paper, we aim to design an arbitrary-order broadband differentiator based on the DLP method. There are three key features of the differentiator: 1) it has an arbitrary magnitude response with a controllable bandwidth; 2) it is different from the technique demonstrated in [11,12] which requires an extra PS-FBG or an LPG-based first-order differentiator to realize a π phase shift for an odd-order differentiation, the proposed differentiator can be designed and fabricated to have an arbitrary differentiation order that is realized in a single FBG; 3) the required maximum index modulation of the FBG-based differentiator can be largely decreased by using a Gaussian windowing function to implement apodization of a target reflection spectrum.

The remainder of this paper is organized as follows. The design of an FBG-based temporal differentiator based on the DLP algorithm is described in Section 2. In Section 3, temporal differentiators with a differentiation order up to the fourth and with a bandwidth up to 500 GHz are designed. A proof-of-concept experiment is carried out in Section 4. A first-order and a second-order temporal differentiators with a bandwidth of 25 GHz are experimentally demonstrated. A conclusion is drawn in Section 5.

2. Principle

An N^{th} -order photonic temporal differentiator is a device that performs the N^{th} -order time derivative of the complex temporal envelope of an input optical waveform. For an optical signal with a central frequency ω_0 (i.e., optical carrier frequency) and a complex envelope $e(t)$, the spectrum of the signal represented in the Fourier domain can be expressed as $E(\omega - \omega_0)$, where ω is the optical frequency. An N^{th} -order temporally differentiated signal with an envelope of $\partial^N e(t) / \partial t^N$ has a frequency response given by

$$r(\omega) = [j(\omega - \omega_0)]^N E(\omega - \omega_0). \quad (1)$$

Therefore, an N^{th} -order temporal differentiation can be implemented by using a filter that provides a spectral transfer function of the form $[j(\omega - \omega_0)]^N$. For an N^{th} even-order differentiator based on an FBG in reflection, the magnitude of the reflection spectrum should be dependent on $(\omega - \omega_0)^N$, and moreover it should provide a zero reflection at the carrier frequency ω_0 . For the N^{th} odd-order differentiator, an exact π phase shift should be imposed on the reflection spectrum of the filter at the carrier frequency ω_0 .

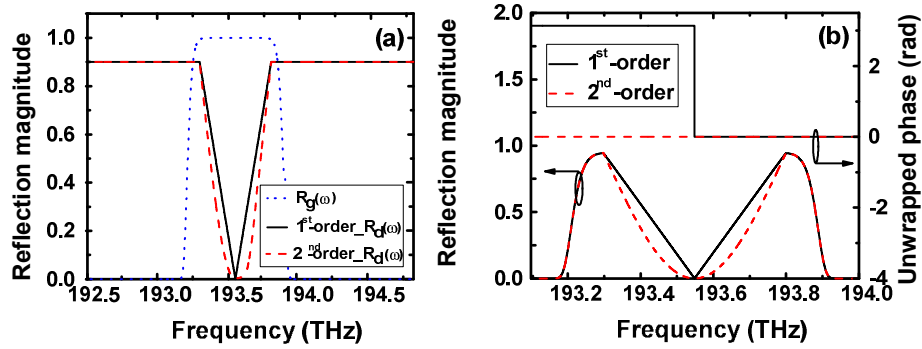


Fig. 1. (a) The high-order Gaussian spectrum $R_g(\omega)$ and the reflection spectra $R_d(\omega)$ used to implement the first-order and the second-order differentiation; (b) The formed target reflection magnitude and phase responses of the first-order and the second-order differentiator.

The principle of the DLP method is based on the solutions of the coupled mode equations with piece-wise scattering and propagation matrix. To design an FBG based on the DLP method, one should build a reflection spectrum used as an ideal target function. Figure 1 shows the formation of the target reflection and its unwrapped phase spectra of a first-order and a second-order temporal differentiator. It is well known that the coupling coefficient of a weak FBG approximately equals to the Fourier transform of its reflection spectrum. Based on Parseval's theorem, we have

$$\int_{-\infty}^{+\infty} \left| \frac{1}{2} q \left(\frac{z}{2} \right) \right|^2 dz = \int_{-\infty}^{+\infty} |r(\delta)|^2 d\delta, \quad (2)$$

where q is the coupling coefficient of the FBG, r denotes the reflection spectrum, z is a local distance along FBG and δ is a normalized frequency detuning from the central Bragg reflection frequency [13]. Based on Eq. (2), we deduce that the integral of the spectrum of an apodized FBG is smaller than the integral of the spectrum of the same un-apodized FBG. Thus, the apodization of a target reflection spectrum can be used to decrease the required coupling coefficient (i.e., the maximum coupling coefficient). To this aim, we form the target reflection spectrum by multiplying a high-order Gaussian spectrum expressed as

$$r_g(\omega) = R_g(\omega) = A \exp(-\omega^{2n} / \sigma^{2n}), \quad (3)$$

with the ideal differentiator spectrum

$$r_d(\omega) = R_d(\omega) \exp[-j\phi(\omega)], \quad (4)$$

where $R_g(\omega)$ and $R_d(\omega)$ are the magnitude spectra of $r_g(\omega)$ and $r_d(\omega)$, respectively, and $\phi(\omega)$ denotes the phase of the spectrum $r_d(\omega)$.

The dotted line (blue) in Fig. 1(a) shows the reflection magnitude $R_g(\omega)$ of the high-order Gaussian spectrum. The spectra of the reflection magnitude $R_d(\omega)$ used to implement the first-order [solid line (black)] and second-order [dash line (red)] differentiation are also illustrated in Fig. 1(a). The central frequencies of the three spectra are all 193.55 THz (i.e., 1550 nm in the wavelength domain). The two spectra $R_d(\omega)$ have the same bandwidth and maximum reflectivity which are 500 GHz and 90%, respectively. The maximum reflectivity of the high-order Gaussian spectrum is 100%. Since the target reflection spectrum $r(\omega)$ can be expressed as

$$r(\omega) = r_g(\omega)r_d(\omega) = R_g(\omega)R_d(\omega)\exp[-j\phi(\omega)], \quad (5)$$

the FBG to be designed has a reflectivity and a bandwidth of 90% and 500 GHz, and the central frequency is identical to that of the spectrum $r_d(\omega)$ (i.e., 193.55 THz), as can be seen from Fig. 1(b). Since no π phase shift is required in a second-order differentiator, the value of its phase is a constant over the whole band, as can be seen from the upper dashed line (red) in Fig. 1(b). It is different from a second-order differentiator, to implement a first-order differentiation, a π -phase shift should be introduced to the phase response of the reflection spectrum at the frequency ω_0 , as it is shown by the upper solid line (black) in Fig. 1(b).

It is worth noting that the design principle determines the features of the proposed arbitrary-order differentiator. Since the π -phase shift and the reflection spectrum are designed separately, the bandwidth is controllable and the magnitude response can be arbitrary. Note that once the differentiator is designed and fabricated, its bandwidth and differentiation order are not changeable. In addition, the odd-order differentiation can also be realized in a single FBG without the need of an additional FBG for the introduction of the π phase shift.

3. Design examples

As illustrated in Fig. 2(a) and (b), by applying the DLP method, the index modulations of the first-order and the second-order differentiators are obtained based on the target reflection spectra with Gaussian apodization. The maximum index modulations of the first-order and the second-order differentiators are 2.0×10^{-3} and 1.7×10^{-3} which can be fabricated in hydrogen loaded single-mode fiber with the conventional phase-mask-based FBG writing technique using a continuous-wave (CW) ultra-violet (UV) light source or the infrared femtosecond pulse writing technique [21]. The insets in Fig. 2 give zoom-in views of the index modulation profiles. It can be seen that the period of both the index modulation profiles in Fig. 2(a) and (b) are about 0.2 mm. An effective controlling resolution of the writing beam position in a range of tens of micrometer will be enough to control the index profile in fabricating the FBGs.

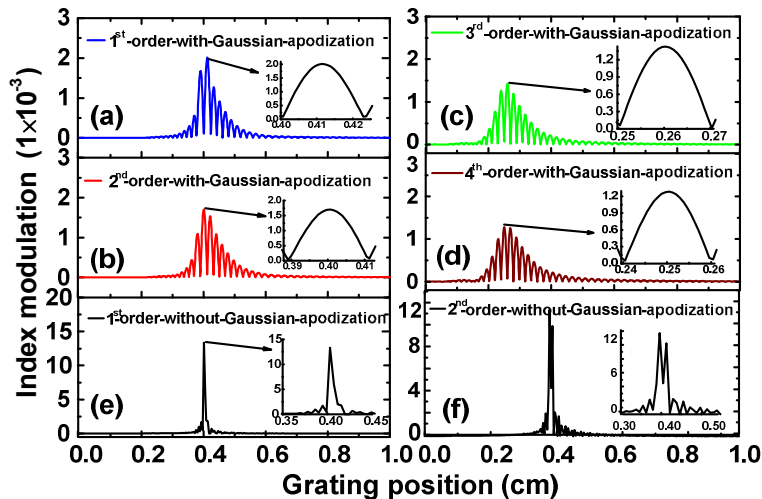


Fig. 2. Index modulation profiles of the synthesized FBGs for the implementation of (a) the first-order differentiator, (b) the second-order differentiator, (c) the third-order differentiator and (d) the fourth-order differentiator based on the reflection spectra with Gaussian apodization in Fig. 1(b). Index modulation profiles for (e) the first-order differentiator and (f) for the second-order differentiator which are synthesized from the reflection spectrum without Gaussian apodization [see Fig. 1(a)].

To demonstrate the capability of designing high-order temporal differentiators, a third-order and a fourth-order temporal differentiator are also designed based on the same design strategy. The index modulation profiles of the two differentiators are shown in Fig. 2(c) and (d). The peak index modulations of the third- and fourth-order differentiators are 1.4×10^{-3} and 1.2×10^{-3} , respectively. As can be seen a higher order differentiator has a lower peak index modulation, which can also be explained from Fig. 1(b) and Eq. (2). The value of the right-hand side of Eq. (2) will be smaller for a higher-order differentiator (i.e., the second-order differentiator).

On the other hand, as shown in Figs. 2(e) and (f), the index modulations of the synthesized first- and second-order differentiators based on the reflection spectrum without Gaussian apodization are respectively about 14×10^{-3} and 12×10^{-3} which are much higher than the index modulation with Gaussian apodization. For an FBG with high index modulation, the fabrication becomes difficult. Therefore, the use of Gaussian apodization on the reflection spectrum is a good design strategy to reduce the index modulation, which is one of the key advantages of the proposed technique.

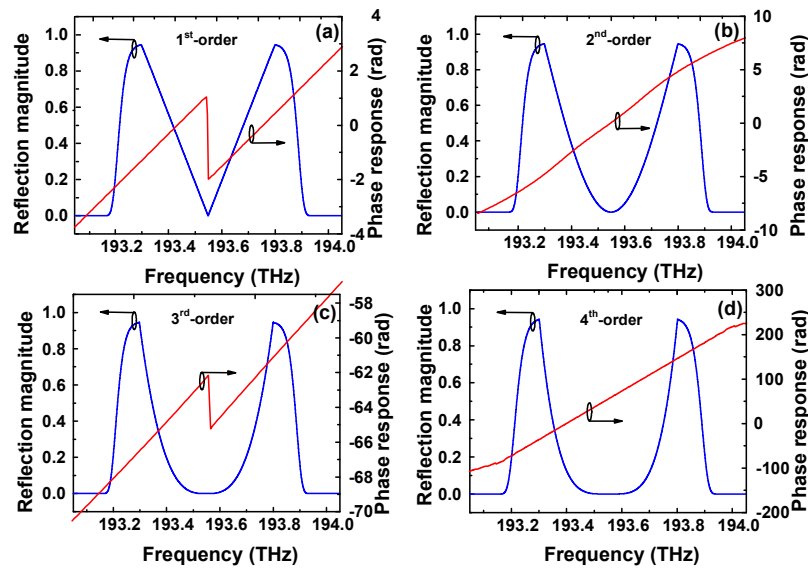


Fig. 3. Reflection magnitude and phase responses of the synthesized FBGs for (a) the first-order differentiator, (b) the second-order differentiator, (c) the third-order differentiator, and (d) the fourth-order differentiator.

Figure 3(a)-(d) shows the simulated reflection magnitude and phase responses of the synthesized FBGs in Fig. 2(a)-(d). As can be seen from Fig. 3(a), an inverted triangular magnitude response is generated for the first-order differentiator. A π phase shift is also realized at the optical frequency ω_0 . Since there exists a constant group delay due to the length of the optical fiber, the simulated unwrapped phase is not constant but linearly increasing. Again, from Fig. 3(b) we can see the FBG with a quadratic reflection magnitude is also successfully realized for the second-order differentiator. As expected, there is no any phase shift in the entire band. Since the desirable magnitude and phase responses are obtained over the entire bandwidth, both the first- and the second-order differentiators have an effective bandwidth of 500 GHz. Figure 3(c) and (d) also show a good agreement between the target and the simulated magnitude and phase responses.

To confirm that the designed FBGs can operate as a first-order and a second-order temporal differentiator, a Gaussian pulse with a bandwidth of 500 GHz is directed into the two designed FBGs. As shown in Fig. 4(a), an output pulse is generated by the first-order differentiator and the generated pulse is in agreement with an ideal first-order differentiated

pulse. Figure 4(b)-(d) shows the results for the second-, third- and fourth-order differentiators. Again, the simulated output pulses also agree well with the ideal differentiated pulses.

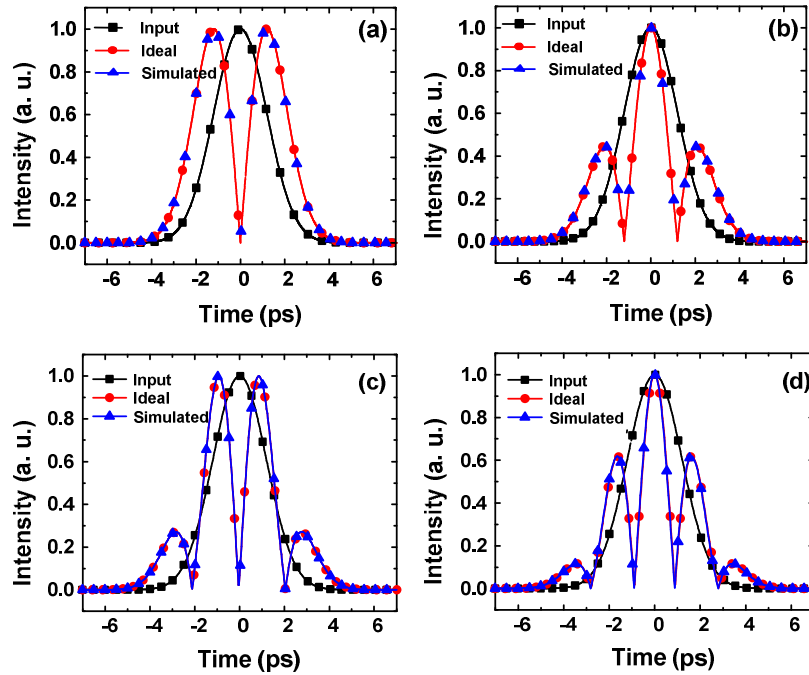


Fig. 4. Output pulse obtained from an input Gaussian pulse with a bandwidth of 500 GHz applied to (a) the first-order differentiator; (b) the second-order differentiator; (c) the third-order differentiator, and (d) the fourth-order differentiator.

4. Proof-of-concept experiment

A proof-of-concept experiment is then carried out to further verify the proposed technique. The experimental setup is shown in Fig. 5, which consists of a tunable laser source (TLS), a polarization controller (PC), an electro-optic intensity modulator (IM), an optical circulator, an erbium-doped fiber amplifier (EDFA), a photodetector (PD), a sampling oscilloscope (SC), and a bit error rate tester (BERT). The TLS is used as an optical source to produce a CW optical carrier which has a wavelength tunable range from 1520 to 1620 nm and a wavelength resolution of 1 pm. The CW light wave from the TLS is directed to the IM. An electrical Gaussian-like pulse train with a bit rate of 13.5 Gbit/s is generated by the BERT (Agilent 4901B) and drives the IM. The pulse shape is close to a Gaussian with an adjustable full-width at half-maximum (FWHM) that in our experiments was kept around 63 ps. The optical Gaussian-like signal is connected to the FBG-based temporal differentiator through an optical circulator (OC). The differentiated pulse is amplified by an EDFA and then detected by a 53-GHz PD with its waveform observed by a high speed SC (Agilent 86116A).

Since the maximum bit rate of the available BERT is only 13.5 Gbit/s, we decrease the bandwidth of the temporal differentiator from 500 to 25 GHz in the proof-of-concept experiment. The temporal differentiator is designed to have a bandwidth of 25 GHz by using the above introduced method. The FBG is then fabricated by a frequency-doubled argon-ion laser operating at 244 nm using a uniform phase mask. The apodization is obtained by dephasing the subsequent exposures while the UV beam is scanning the mask with a technique similar to that reported in [22]. The index modulations of the designed 25-GHz first-order and second-order temporal differentiators are illustrated in Fig. 6(a) and (b). It can be seen that the peak index modulations are about 1×10^{-4} for both differentiators, which is much lower than

the ones with a bandwidth of 500 GHz. Moreover, the periods of the index modulations are about 0.40 cm for both differentiators which make the fabrication of the differentiators easier. In other words, with the increase of the bandwidth, the index modulation of the temporal differentiator will become too complex to be practically fabricated. This characteristic may be considered as a main limitation of the proposed method.

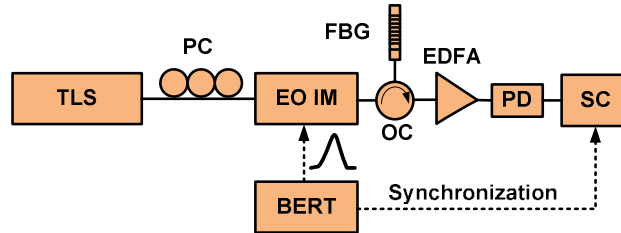


Fig. 5. Experimental setup. TLS, tunable laser source; PC, polarization controller; EO IM, electro-optic intensity modulator; OC, optical circulator; EDFA, erbium-doped fiber amplifier; PD, photodetector; SC, sampling oscilloscope; BERT, bit error rate tester.

For comparison, the simulated and the measured reflection spectra of the fabricated first-order and second-order temporal differentiator are shown in Fig. 7. It can be seen from Fig. 7(a) and (b) a good agreement between the simulated spectra of the first- and second-order differentiators with the measured reflection spectra is achieved in a region wider than 25 GHz around the central Bragg frequency. The insets of the Fig. 7(a) and (b) illustrate the phase responses of the first- and second-order differentiators which are measured by an optical vector analyzer (Luna Technologies). The anticipated π phase shift at the central wavelength of the first-order differentiator is observed. The phase response of the second-order differentiator is linearly increasing which agrees well with the target phase response.

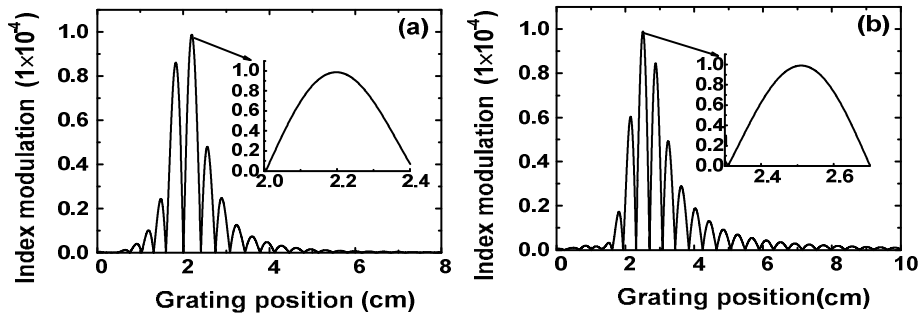


Fig. 6. Index modulation of the designed 25 GHz (a) first-order differentiator and (b) second-order differentiator.

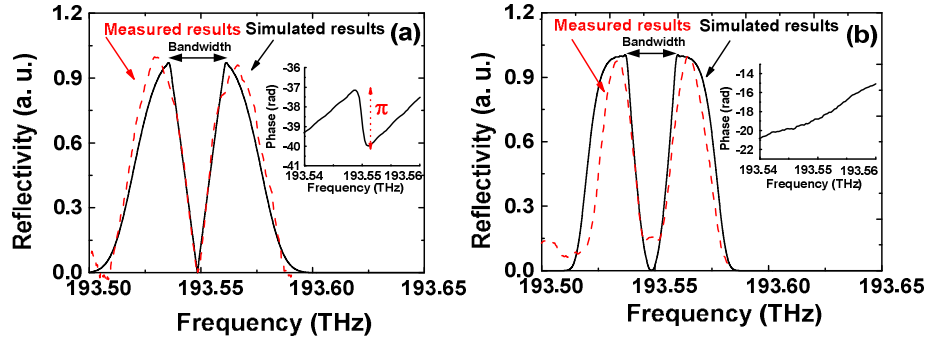


Fig. 7. Simulated (solid line) and measured (dashed line) reflection spectra for (a) the first-order differentiator and (b) the second-order differentiator. The insets show the phase responses of the differentiators.

The input and the output pulses of the first-order temporal differentiator are shown in Fig. 8. Figure 8(a) shows the simulated and the measured input Gaussian-like pulse. The intensities of the corresponding first-order differentiated pulses are illustrated in Fig. 8(b). It can be seen that the measured differentiated pulse fits well with the simulated pulse except a small discrepancy in the central part of the pulse. The average deviation between two pulses is about 10.3%. We believe that the deviation is due to the asymmetry of the input pulse generated by the BERT [see the dashed line in Fig. 8(a)]. As for the second-order differentiator, since the input pulse shown in Fig. 9(a) is quite symmetrical, the simulated and the measured second-order differentiated pulses match very well, as can be seen from Fig. 9(b). Here, the average deviation between the simulated and the measured waveform is as small as 3.1%.

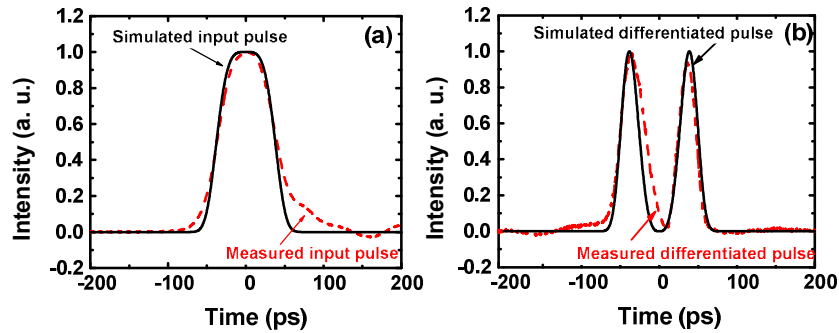


Fig. 8. Input and output pulses for the first-order temporal differentiator. (a) Simulated and measured input pulses; (b) Simulated and measured output pulses.

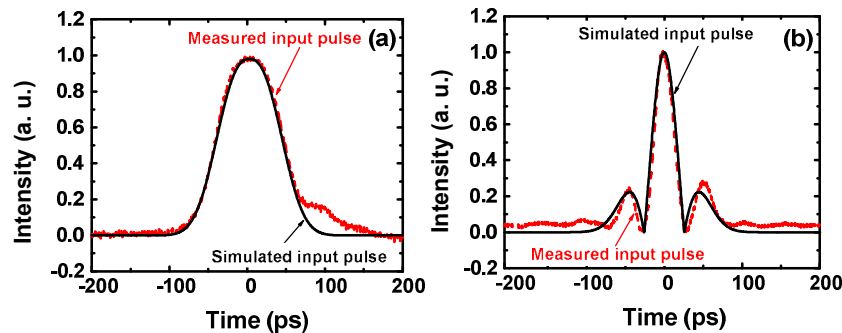


Fig. 9. Input and output pulse of the second-order temporal differentiator. (a) Simulated and measured input pulses; (b) Simulated and measured output pulses.

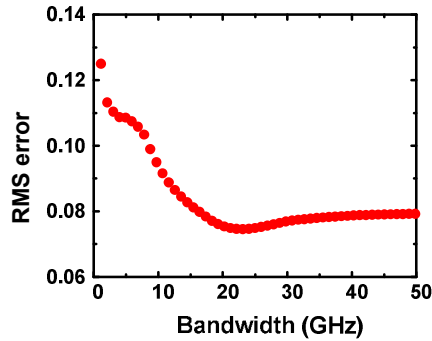


Fig. 10. Estimated processing error as a function of the input pulse bandwidth for the fabricated second-order differentiator. RMS: root mean square.

Finally, the processing error as a function of the input pulse bandwidth is investigated. As an example, the fabricated second-order differentiator is employed to estimate the processing error [11,12] for an input Gaussian pulse with different bandwidth. To do so, we first measure the spectral response of the fabricated second-order differentiator using the Luna optical vector analyzer, and then to calculate the output pulse for an input Gaussian pulse with different bandwidth. The processing error is then obtained by calculating the root mean square (RMS) error for the Gaussian pulse with a bandwidth from 0 to 50 GHz, with the results shown in Fig. 10. As can be seen there exists an optimal operation bandwidth where the RMS error is minimized. In general, the performance of the fabricated second-order FBG is poorer for an input signal with a narrower bandwidth.

5. Conclusion

A new technique to design and implement an arbitrary-order all-optical temporal differentiator was proposed and experimentally demonstrated. By controlling the magnitude and phase responses of an FBG designed based on the DLP method, a temporal differentiator with an arbitrary differentiation order and a controllable bandwidth in a single FBG was realized. Based on the proposed technique, temporal differentiators with an order up to the fourth and with a bandwidth as large as 500 GHz were designed and analyzed. To verify the design, a first-order and a second-order temporal differentiators were fabricated. The spectral responses of the two fabricated differentiators were then compared with the simulated spectral responses, and an excellent agreement was achieved. The use of the first- and second-order differentiators to generate differentiated waveform for an input Gaussian pulse was performed. Again, excellent results were obtained. The average deviations between the simulated and measured temporal waveforms of the first-order and the second-order differentiators were estimated to be about 10.3% and 3.1%, respectively.

Acknowledgments

This work was supported by The Ontario Centres of Excellence (OCE), Canada, and The Institut de Ciències Fotòniques (ICFO), Spain. We would also like to acknowledge partial support from the Spanish National Programs Plan Nacional No. TEC2007-60185 and Juan de la Cierva.